Triangular lattice atomic layer of Sn(1 × 1) at graphene/SiC(0001) interface

Hayashi, Shingo
Department of Applied Quantum Physics and Nuclear Engineering, Kyushu University

Visikovskiy, Anton
Department of Applied Quantum Physics and Nuclear Engineering, Kyushu University

Kajiwara, Takashi
Department of Applied Quantum Physics and Nuclear Engineering, Kyushu University

Iimori, Takushi
The Institute for Solid State Physics, The University of Tokyo

他

出版情報：Applied Physics Express. 11 (1), pp.015202-, 2017-12-21. IOP Publishing
バージョン：

Triangular lattice atomic layer of Sn (1×1) at graphene/SiC(0001) interface

Shingo Hayashi[1], Anton Visikovskiy[1], Takashi Kajiwara[1], Takushi Iimori[2], Tetsuroh Shirasawa[3], Kan Nakastuji[4], Toshio Miyamachi[2], Shuhei Nakashima[2], Koichiro Yaji[2], Kazuhiko Mase[5,6], Fumio Komori[2], Satoru Tanaka[1]*

[1]*Department of Applied Quantum Physics and Nuclear Engineering, Kyushu University, Fukuoka, Fukuoka 819-0395, Japan*
[2]*The Institute for Solid State Physics, The University of Tokyo, Kashiwa, Chiba 277-8581, Japan*
[3]*National Metrology Institute of Japan, National Institute of Advanced Industrial Science and Technology, Tsukuba, Ibaraki 305-8565, Japan*
[4]*Department of Materials Science and Engineering, Tokyo Institute of Technology, Yokohama, Kanagawa 226-8502 Japan*
[5]*Institute of Materials Structure Science, High Energy Accelerator Research Organization (KEK), Tsukuba, Ibaraki 305-0801, Japan*
[6]*Department of Materials Structure Science, SOKENDAI (The Graduate University for Advanced Studies), Tsukuba, Ibaraki 305-0801, Japan*

Sn atomic layers attract great interest towards spin related physical properties due to strong spin-orbit interactions. We performed Sn intercalation into the graphene/SiC(0001) interface and found a new type of Sn atomic layer. Sn atoms occupy on-top sites of Si-terminated SiC(0001) with in-plane Sn-Sn bondings, resulting in a triangular lattice. Angle-resolved photoemission spectroscopy revealed characteristic dispersions at $\bar{K}$ and $\bar{M}$ points, which are in good agreement with DFT calculations. Note the Sn triangular lattice atomic layer at the interface showed no oxidation by exposing to the air, that is significantly useful in characterization and device fabrication *ex situ*.

Since the fabrication of graphene by Geim *et al*,[1)] a lot of attention is concentrated on two-dimensional (2D) group-IV materials: silicene,[2–6)] germanene,[7–11)] and stanene.[12–16)] In particular, stanene is expected to exhibit such unique characteristics as a 2D quantum spin Hall state with large bandgap,[12,13)] topological superconductivity,[14)] and quantum anomalous Hall effect at nearly room temperature.[15)] Experimentally, the formation of stanene on Bi_2Te_3(111) has been reported.[16)] Sn was found to form buckled honeycomb lattice by scanning tunneling microscopy (STM). A larger buckling ($\sim$ 1.2 Å) compared with a calculation for free-standing stanene is introduced by a smaller lattice constant (4.383 Å) of the substrate. In addition, electronic structure measured by angle-resolved photoemission spectroscopy (ARPES) near the $\bar{\Gamma}$ point coincides with the calculations, but no Dirac cone at the $\bar{K}$ point was observed.

On the other hand, magnetic properties of Sn layers are interesting because Sn has a large spin-orbit interaction (SOI). There are reports on the electronic structure and magnetism of adsorbed Sn-($\sqrt{3} \times \sqrt{3}$)R30° (hereinafter, referred to as R3) on Si(111)[17)] and Ge(111).[18)] In these papers, Mott insulator transition at low temperature was observed. Sn adsorption on SiC(0001) is more interesting because the SiC lattice constant is smaller than those of Si and Ge, so stronger SOI is expected and accordingly larger energy gap ($\sim$ 2 eV) between spin-split states is produced. Also, Sn electron correlation effects are more pronounced due to weaker screening owing to a wide band-gap of SiC. These were reported by Glass *et al*.[19)] The insulating ground state of R3-Sn overlayer on SiC(0001) is, however, a subject of intense discussion whether it originated from Mott-type by strong Coulomb repulsion or Slater-type by long distance antiferromagnetic order.[19–21)] The triangular structure of R3-Sn is also a good model system to study spin frustration, possible spin liquid phase formation, and spontaneous magnetic ordering.[22,23)]

Intercalation of various elements into the graphene/SiC interface has been a hot topic in recent years. We found that intercalated Si forms reconstructions different from those formed by adsorbed Si on the surface at low Si coverages.[24)] By analogy, we expect similar behavior of Sn, since the interface is a confined space and promote growth of 2D structures. Another useful feature of this approach is that the Sn layer at interface is protected by graphene against atmosphere exposure. This is advantageous for *ex situ* measurements and electronic applications. Moreover, the intercalated layer may inject polarized spins into graphene,[26,27)] where long spin coherence length and high carrier mobility is expected.[25)] This would give rise to spintronic devices. Actually, gold intercalation induces $\sim$ 100 meV spin splitting in graphene.[28)] The splitting energy strongly depends on the positional relationship between the graphene and the gold atoms, so the structure of the interface may play crucial role in graphene's properties. In this paper, Sn intercalation is attempted at the interface between the graphene buffer layer ($(6\sqrt{3} \times 6\sqrt{3})$R30° structure, hereinafter referred to as 6R3) and the SiC substrate to survey Sn interlayer structure and correlations to electronic structures.

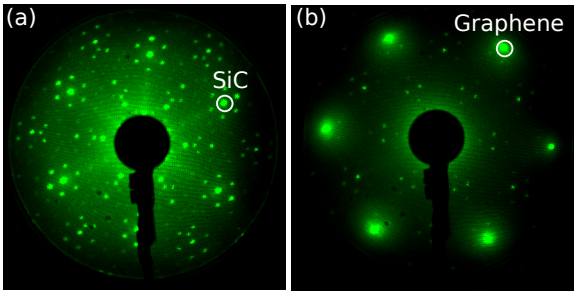

Fig. 1. LEED patterns taken at 60 eV incident beam energy: (a) 6R3 diffraction pattern before Sn deposition, (b) graphene, (1×1), and weak 6R3 diffraction patterns after deposition of Sn and annealing at 700°C. (b) suggests transformation of the 6R3 buffer layer to graphene by Sn intercalation.

*E-mail: stanaka@nucl.kyushu-u.ac.jp

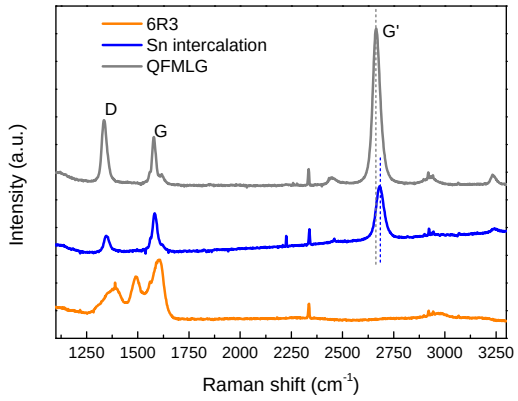

Fig. 2. Raman spectra of the 6R3 buffer layer (red line), the Sn intercalated graphene (blue line), and reference QFML graphene (gray line). G' band appears after Sn intercalation and decoupling of the 6R3 buffer layer. G' peak position of the Sn intercalated sample is slightly blue shifted relative to of the QFMLG sample.

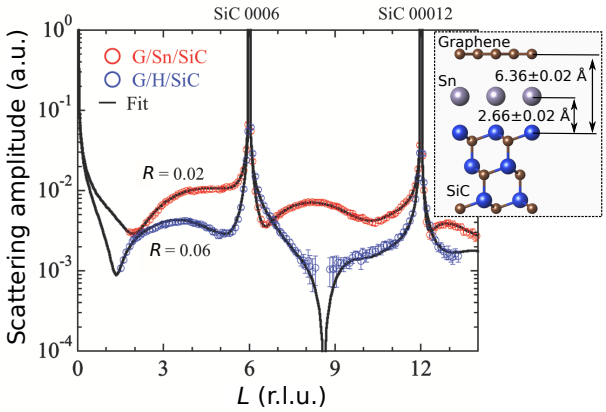

Fig. 3. X-CTR scattering profiles of the Sn intercalated graphene (red circles) and QFMLG (blue circles). Solid lines show fitting data based on the QFMLG model[37] and the Sn intercalated model shown in the inset.

6H-SiC(0001) substrates (on-axis, Si face) were used in this experiment. After etching by hydrogen gas the SiC substrate showed atomically flat surfaces with silicate R3 structure on top.[29] The sample was introduced into the ultra-high vacuum (UHV) chamber and was annealed at 1120°C to decompose the silicate layer, resulting in adatom R3-Si structure.[30] A graphene buffer layer, 6R3, was then prepared by annealing at 1250°C in UHV for 25 minutes.[31,32] Sn was supplied on the surface at the room temperature until the reflection high-energy electron diffraction (RHEED) pattern got cloudy (formation of amorphous layer). The sample temperature was finally raised to about 700°C. During this process the (1×1) RHEED pattern reappeared, graphene and weak 6R3 superreflexes were also observed. This means that part of Sn atoms was intercalated into the 6R3/SiC interface and 6R3 was transformed to graphene. This procedure was repeated until the 6R3 diffraction pattern fainted. For the reference, a quasi-free-standing monolayer graphene (QFMLG) sample was also prepared by hydrogen intercalation performed at 700°C in H_2 gas at atmospheric pressure.[33] The samples were finally evaluated by *in situ* low-energy electron diffraction (LEED), *ex situ* X-ray crystal truncation rod (X-CTR) scattering, Raman spectroscopy, X-ray photoemission spectroscopy (XPS), and ARPES. The atomic structure and energy band dispersions of the Sn interface layer based on the proposed model were investigated by density functional theory (DFT) calculations using VASP code.[41]

The LEED pattern of initial well-ordered 6R3 is shown in Fig. 1(a) with bright and clean superreflexes. Upon annealing of the Sn deposited sample the LEED pattern changes to one shown in Fig. 1(b). Graphene spots significantly increased in intensity, suggesting decoupling of the 6R3 buffer layer induced by Sn intercalation at the 6R3/SiC interface. Besides graphene spots, both LEED and RHEED show clear (1×1) reflexes, which suggests the formation of the (1×1)-Sn interface structure. Some weak 6R3 spots are still visible in LEED pattern in Fig. 1(b). This is probably originated from either residual 6R3 structure (spatially unintercalated area) and/or the 6R3 layer partially modified by Sn atoms (as can be evidenced from the change in spot intensity distribution compared to initial 6R3 pattern taken at the same energy).

Decoupling of the buffer layer and transformation to monolayer graphene has also been confirmed by *ex situ* Raman spectroscopy as seen in Fig. 2, where spectra from initial 6R3, Sn intercalated and QFMLG samples are shown. The spectrum of the Sn intercalated sample indicates no characteristic features of 6R3 structure[35] and pronounced graphene related G' (2682 cm^{-1}), G (1583 cm^{-1}), and D (1348 cm^{-1}) peaks appear. From G- and G'-band peak position it is possible to estimate carrier density and in-plane stress of monolayer graphene,[36] which are $< 10^{12} cm^{-2}$ and $\approx 0.1\%$, respectively. This estimated carrier density is in agreement with ARPES results (Fig. 6) and will be discussed below.

To evaluate the interfacial structure of the Sn intercalated sample X-CTR scattering measurement, a very precise analysis for measuring an interlayer distance and a density of each layer, was carried out. A QFMLG sample was also provided for comparison. The profiles from both samples are shown in Fig. 3. The profile of the Sn intercalated sample was best fitted with the (1×1) model, Sn atoms positioned at T_1 sites on SiC(0001) surface at the graphene/SiC interface with structure parameters shown in the inset of Fig. 3. The reliability factor R is 0.02, which is very small (good agreement), considering R=0.06 for the hydrogen intercalated sample using the structural model already identified.[37] The determined Sn-Si interlayer distance is 2.66±0.02 Å, which agrees with that obtained by the DFT calculations for the Sn on the T_1 site model. The derived areal occupancies of Sn (assuming (1×1) structure with 1 ML nominal coverage) and graphene layers to SiC(0001) surface are 0.63±0.02 and 0.73±0.03, respectively, which are reasonably close so that decoupled graphene layer mostly sits ontop of the Sn layer. The discrepancy in occupation comes from the existence of small portion of partially intercalated regions. The Sn layer is found to be perfectly flat without any noticeable buckling. The interlayer distance between graphene and Sn layer is $\approx$ 3.7 Å, which is 1 Å larger than that of hydrogenated sample and equals to the sum of van-der-Waals radii of Sn and C, indicating weak coupling to graphene, as expected.

The results of XPS measurements performed after exposing sample to the atmosphere and annealing at 500°C in UHV are shown in Fig. 4. Only Si, C, and Sn peaks are prominent in the spectrum by wide-range scan (Fig. 4(a)). Almost no O

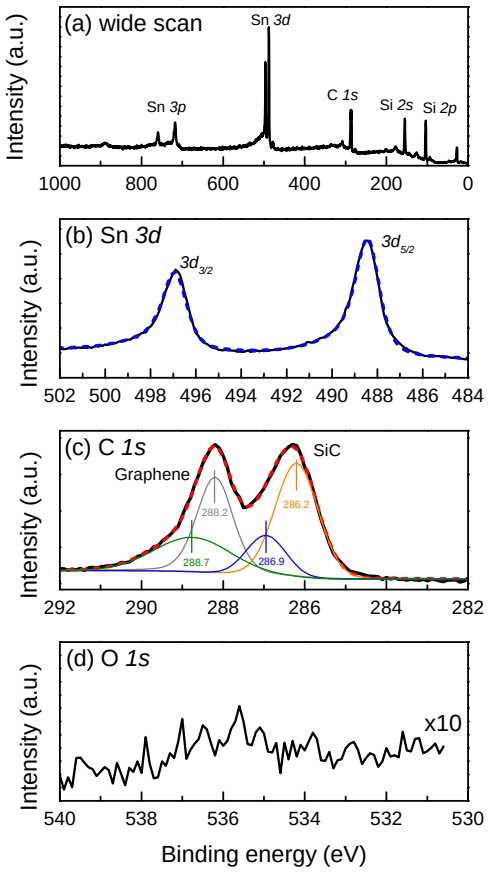

Fig. 4. XPS data of Sn intercalated graphene: (a) wide-scan; (b) Sn 3*d* core level; (c) C 1*s* core level (see discription of each component in main text); (d) O 1*s* core level. Sn 3*d* is fitted with a single component (dashed blue line), indicating all Sn atoms at the interface are in the identical chemical environment. No O 1*s* signal is detected. This means the sample is not oxidized by atmospheric exposure.

1*s* peak is visible (see Fig. 4(d) for a magnified energy range), which indicates that the Sn interface layer is not oxidized and is protected by graphene, making this kind of structure robust for device applications and scientific analyses with variety of *ex situ* methods. Sn 3*d* peak (Fig. 4(b)), fitted by the asymmetric Gaussian-Lorentzian sum function[38] often used in metals, exhibits single component corresponding to Sn atoms being in identical chemical environment. This is consistent with the proposed (1×1) interface layer model as shown in the inset of Fig. 3. In Fig. 4(c) C 1*s* spectrum is presented and analyzed using symmetrical Gaussian-Lorentzian product functions. It consists of two main prominent peaks related to sp^3 bonded C of bulk SiC (286.2 eV) and sp^2 bonded C of graphene (288.2 eV). Each peak can be decomposed into two components. The components with lower binding energy (orange and gray lines) are assigned to bulk SiC under Sn interface layer (286.2 eV) and decoupled graphene (288.2 eV), respectively. The higher binding energy components (blue and green lines) are due to the remaining 6R3 (as observed by LEED) phase, which is known to introduce surface band bending owing to surface charge formation.[39] The "sp^2" 6R3 component (288.7 eV) is relatively wide and contains contribution from remaining ordinary 6R3 as well as from one partially intercalated by Sn. The area ratio of peaks corresponding to decoupled graphene (gray) and 6R3 (green) is 7 : 3, which is in good agreement with the area ratio obtained by the X-CTR scattering profile.

Electronic structure of the graphene/Sn/SiC sample was investigated by ARPES. In Fig. 5(a), photoemission intensity mapping in k-space and theoretical dispersion curves by the DFT calculations are shown. The DFT calculations are based on the SiC(0001)-(1×1)-Sn structural model depicted in Fig. 5(b). Graphene is not included in this calculation due to limited computational capability (too large overall unit cell) and decoupled nature of graphene. Total energy calculations show that T_1 on-top adsorption site (Fig. 5(b)) for Sn is by far ($>$ 0.3 eV per unit cell) more preferable than the other sites such as T_4 and H_3. Details will be published elsewhere.

Overall, the calculated bands are in excellent agreement with the results of ARPES. Several notable features can be recognized by comparing the ARPES data with the calculated bands. There are three surface bands: S_1, S_2 and S_3 as indicated in Fig. 5(a). Bottom of the S_1 band at $\bar{K}_{1\times1}$ point is very close to the Fermi level (E_F). The S_2 and S_3 bands exhibit cone-like shapes at $\bar{K}_{1\times1}$ point around -1.6 eV. The two cone branches are separated by a small gap of 150 meV in the calculation results. However, the gap was not clearly observed in the experiment because of weak ARPES signals in this area. The S_3 band runs across almost the whole Brillouin zone (BZ) and merges into the hole-like parabolic bands near $\bar{\Gamma}$ point, which are the top of the bulk valence band of SiC. In the figure, red-marked areas of the bands are assigned to the Sn p_z states which are hybridized with Si dangling bonds, whereas cone-like bands (yellow-marked) are due to in-plane Sn-Sn bonds originating from $p_x + p_y$ orbitals. These results certify that a triangular lattice atomic layer (TLAL) consisting of Sn is formed at the interface. Furthermore, calculations including SOI shows strong spin polarization in the S_1, S_2 and S_3 bands (not shown). Hence, spin injection into graphene can be expected, making this system interesting for spintronics device applications. The results of spin-resolved ARPES will be reported elsewhere.

A Dirac cone of top graphene layer was observed along $\bar{\Gamma}$-$\bar{K}_G$-$\bar{M}_G$ at $\bar{K}_G$ point, as shown in Fig. 6. A Dirac point is located at $\simeq E_F$, indicative of the significantly low carrier concentration, that gives reasonable agreement with the Raman analysis. This result is considered by comparing with the reference of a hydrogen-intercalated QFMLG sample, which exhibits a Dirac point at 0.1 eV above E_F. This p-doping behavior is explained by spontaneous polarization of hexagonal SiC substrate.[40] As the Sn interface layer is metallic as shown by ARPES, most probably it screens SiC polarization dipoles from graphene resulting in non-doped graphene layer. In addition, interestingly, replica Dirac cone could be observed at 0.7 Å^{-1} point along $\bar{\Gamma}$-$\bar{K}_G$ direction. This replica is induced by (1×1) periodicity of the interface (see the inset of Fig. 6). The replicas due to graphene BZ are also seen for the Sn derived bands, indicated by dashed cyan lines in Fig. 5(a).

In conclusion, we intercalated Sn atoms into the graphene/SiC interface. Sn intercalation decoupled a 6R3 buffer layer and transformed it into a non-doped free-standing graphene. From the structural analyses by LEED and X-ray CTR scattering and also comparison between ARPES observation and DFT calculations it was concluded that the interface structure of Sn layer is a novel (1×1) TLAL exhibiting Dirac-cone like feature in the band structure. Physical prop-

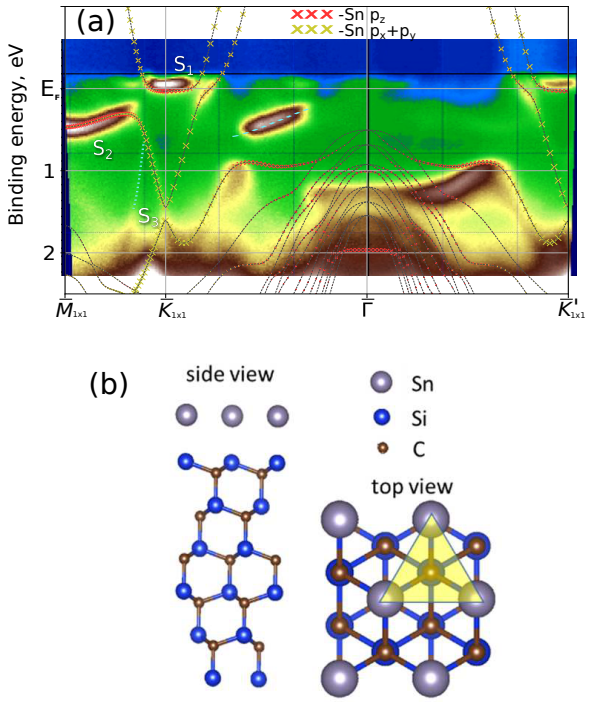

Fig. 5. (a) ARPES intensity map of the Sn intercalated graphene sample overlayed with the calculated band structure by DFT based on the model shown in (b). Contribution of the Sn p_z and $p_x + p_y$ orbitals to the surface (S_1, S_2, S_3) and bulk states is shown with yellow and red crosses, respectively. (b) TLAL model used in the DFT calculations.

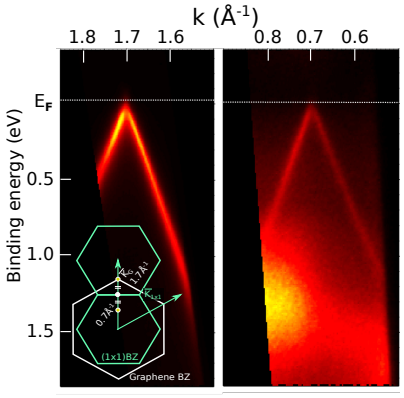

Fig. 6. ARPES intensity map of graphene Dirac cone at $\bar{K}_G$ point (1.7 Å^{-1}) and its replica at 0.7 Å^{-1}. The BZ of SiC(Sn)(1 × 1) and graphene is shown in the inset.

erties of such layers have not been reported so far, but significant spin-polarization of electronic states induced by strong SOI of Sn atoms and topological insulator properties are expected.

The ARPES measurements were partly performed at BL-13B, PF, KEK, Japan (PF-PAC No.2017G575). The X-CTR experiments were performed at PF, KEK, Japan (PF-PAC No.2016G548).

1) K. S. Novoselov, A. K. Geim, S. V. Morozov, D. Jiang, Y. Zhang, S. V. Dubonos, I. V. Grigorieva, and A. A. Firsov, Science 306, 666 (2004).
2) G. G. Guzmán-Verri and L. C. L. Y. Voon, Phys. Rev. B 76, 075131 (2007).
3) B. Lalmi, H. Oughaddou, H. Enriquez, A. Kara, S. Vizzini, B. Ealet, and B. Aufray, Appl. Phys. Lett. 97, 223109 (2010).
4) P. Vogt, P. De Padova, C. Quaresima, J. Avila, E. Frantzeskakis, M. C. Asensio, A. Resta, B. Ealet, and G. Le Lay, Phys. Rev. Lett. 108, 155501 (2012).
5) B. Feng, Z. Ding, S. Meng, Y. Yao, X. He, P. Cheng, L. Chen, and K. Wu, Nano Lett. 12, 3507 (2012).
6) A. Fleurence, R. Friedlein, T. Ozaki, H. Kawai, Y. Wang, and Y. Yamada-Takamura, Phys. Rev. Lett. 108, 245501 (2012).
7) L. Li, S. Z. Lu, J. Pan, Z. Qin. Y. Q. Wang, Y. Wang, G. Cao, S. Du, and H. J. Gao, Adv. Mater. 26, 4820 (2014).
8) M. E. Dávila, L. Xian, S. Cahangirov, A. Rubio, and G. Le Lay, New J. Phys. 16, 095002 (2014).
9) P. Bampoulis, L. Zhang, A. Safaei, R. van Gastel, B. Poelsema, and H. J. W. Zandvliet, J. Phys. Condens. Matter 26, 442001 (2014).
10) M. Derivaz, D. Dentel, R. Stephan, M.C. Hanf, A. Mehdaoui, P. Sonnet, and C. Pirri, Nano Lett. 15, 2510 (2015).
11) L. Ahang, P. Bampoulis, A. N. Rudenko, Q. Yao, A. van Houselt, B. Poelsema, M. I. Katsnelson, and H. J. W. Zandvliet, Phys. Rev. Lett. 116, 256804 (2016).
12) Y. Xu, B. Yan, H. J. Zhang, J. Wang, G. Xu, and P. Tang, Phys. Rev. Lett. 111, 136804 (2013).
13) C. C. Liu, H. Jiang, and Y. Yao, Phys. Rev. B 84, 195430 (2011).
14) J. Wang, Y. Xu, and S. C. Zhang, Phys. Rev. B 90, 054503 (2014).
15) S. C. Wu, G. Shan, and B. Yan, Phys. Rev. Lett. 113, 256401 (2014).
16) F. F. Zhu, W. J. Chen, Y. Xu, C. L. Gao, D. D. Guan, C. H. Liu, D. Qian, S. C. Zhang and J. F. Jia, Nat. Mater. 14, 1020 (2015).
17) S. Modesti, L. Petaccia, G. Ceballos, I. Vobornik, G. Panaccione, G. Rossi, L. Ottaviano, R. Larciprete, S. Lizzit, and A. Goldni, Rhys. Rev. Lett. 98, 126401 (2007).
18) R. Cortes, A. Tejeda, J. Lobo, C. Didiot, B. Kierren, D. Malterre, E. G. Michel, and A. Mascaraque, Phys. Rev. Lett. 96, 126103 (2006).
19) S. Glass, G. Li, F. Adler, J. Aulbach, A. Fleszar, R. Thomale, W. Hanke, R. Claessen, and J. Schäfer, Phys. Rev. Lett. 114, 247602 (2015).
20) S. Yi, H. Lee, J.-H. Choi and J.-H. Cho, Sci. Rep. 6, 30598 (2016).
21) V. I. Anisimov, A. E. Bedin, M. A. Korotin, G. Santoro, S. Scandolo, and E. Tosatti, Phys. Rev. B 61, 1752 (2000).
22) P. W. Anderson, Science 235, 1196 (1987).
23) Y. Shimizu, K. Miyagawa, K. Kanoda, M. Maesato, and G. Saito, Phys. Rev. Lett. 91, 107001 (2003).
24) A. Visikovskiy, S. Kimoto, T. Kajiwara, M. Yoshimura, T. Iimori, F. Komori, and S. Tanaka, Phys. Rev. B 94, 245421 (2016).
25) N. Tombros, C. Jozsa, M. Popinciuc, H. T. Jonkman, and B. J. van Wees, Nature 448, 571 (2007).
26) M. Shiraishi, M. Ohishi, R. Nouchi, N. Mitoma, and T. Nozaki, Adv. Funct. Mater. 19, 3711 (2009).
27) W. Han, K. Pi, W. Bao, K. M. McCreary, Y. Li, W. H. Wang, C. N. Lau, and R. K. Kawakami, Appl. Phys. Lett. 94, 222109 (2009).
28) D. Marchenko, A. Varykhalov, M. R. Scholz, G. Bihlmayer, E. I. Rashba, A. Rybkin, A. M. Shikin, and O. Rader, Nat. Commun. 3, 1232 (2012).
29) J. Bernhardt, J. Schardt, U. Starke, and K. Heinz, Appl. Phys. Lett. 74, 1084 (1999).
30) U. Starke, J. Schardt, J. Bernhardt, M. Franke, and K. Heinz, Phys. Rev. Lett. 82, 2107 (1999).
31) A. J. van Bommel, J. E. Crombeen, and A. van Tooren, Surf. Sci. 48, 463 (1975)
32) K. V. Emtsev, F. Speck, Th. Seyller, L. Ley, and J. D. Riley, Phys. Rev. B 77, 155303 (2008).
33) C. Riedl, C. Coletti, T. Iwasaki, A. A. Zakharov, and U. Starke, Phys. Rev. Lett. 103, 206804 (2009).
34) J. Röhrl, M. Hundhausen, K. V. Emtsev, Th. Seyller, R. Graupner, and L. Ley, Appl. Phys. Lett. 92, 201918 (2008).
35) F. Fromm, M. H. Oliveira Jr., A. Molina-Sánchez, M. Hundhausen, J. M. J. Lopez, H. Riechert, L. Wirtz and Th. Seyller, New. J. Phys. 15, 043031 (2013)
36) J. E. Lee, G. Ahn, J. Shim, Y. S. Lee, and S. Ryu, Nat. Commun. 3, 1024 (2012).
37) J. D. Emery, V. D. Wheeler, J. E. Johns, M. E. McBriarty, B. Detlefs, M. C. Hersam, D. K. Gaskill, and M. J. Bedzyk, App. Phys. Lett. 105, 161602 (2014).
38) S. Hüfner, Photoelectron Spectroscopy (Solid-State Sciences, 1996)

2nd ed., p. 112.
39) W. Chen, S. Chen, Z. H. Ni, H. Huang, D. C. Qi, X. Y. Gao, Z. X. Shen, and A. T. S. Wee, Jpn. J. Appl. Phys. 49, 01AH05 (2010).
40) J. Ristein, S. Mammadov, and Th. Seyller, Phys. Rev. Lett. 108, 246104 (2012).
41) G. Kresse and J. Furthmüller, Phys. Rev. B 54 , 11169 (1996).